Computer Assisted Mechanics and Engineering Sciences, 8: 183–204, 2001.

Simulation of instabilities in non-softening Drucker–Prager plasticity[1]

Anna Stankiewicz and Jerzy Pamin
Faculty of Civil Engineering, Cracow University of Technology,
ul. Warszawska 24, 31-155, Cracow, Poland

(Received January 4, 2000)

The problem of instability and strain localization in a hardening non-associative Drucker–Prager plasticity theory is analyzed. The classical and gradient-enhanced versions of the theory are reviewed and instability indicators are summarized. The regularizing properties of the gradient-enhancement are shown. The classical plane strain biaxial compression test is analyzed in terms of the analytical prediction of ellipticity loss and numerical simulation of the process of shear band formation and evolution. The influence of material model parameters, especially of the degree of non-associativity and the gradient influence, on the instability properties is demonstrated.

1. Introduction

The problem of material instabilities inducing strain localization has been investigated for instance in the review papers [35, 10, 18], in the thorough study of bifurcations in geomaterials [32] and, recently, in the proceedings of IUTAM symposium [11]. If a material instability [13, 15] is encountered in the deformation history of a body, the strains often localize in a number of narrow bands, while the remaining parts of the body unload. Within a classical continuum formulation and for static problems this phenomenon is associated with the loss of ellipticity of the governing partial differential equations. Therefore, discretization methods used to solve the equations may yield mesh-sensitive and hence meaningless results. To overcome this problem, a form of rate-dependent or non-local enhancement of the constitutive model must be adopted [28, 10]. The non-locality may have the form of micropolarity (e.g. [17]), integral averaging (e.g. [5]) or spatial gradient-dependence (e.g. [30]). They all imply the introduction of an internal length parameter in the continuum description.

However, majority of the literature of the problem deals with softening materials and relatively few contributions concern the case of hardening materials with non-symmetric constitutive operators. It was shown already by Rudnicki and Rice [24] that the loss of material stability may be encountered for hardening non-associative plasticity and, unless kinematic constraints prevent it, the loss of ellipticity (discontinuous bifurcation) may consequently occur. The case was then studied in [23, 33, 6, 7, 30, 25, 26, 2, 3], but numerical simulations were usually limited to classical continuum models and in particular to Mohr–Coulomb plasticity. The analysis is more difficult than for the associative case since the spectral properties of non-symmetric operators are more intricate to analyze [36, 29].

This paper reapproaches the problem of localization in non-softening media focusing on the numerical analysis of the well-known pressure-dependent and non-associative Drucker–Prager plasticity model. The model has been used for a large class of geomaterials, although it is by now considered insufficiently realistic. However, the discussion here is limited to qualitative aspects of

[1]The paper was presented at the XIVth Polish Conference on Computer Methods in Mechanics, PCCMM'99, Rzeszów, May 26–29, 1999.

instability phenomena in the form of (a pattern of) shear bands. We limit our consideration to the case of constant values of the friction and dilatancy angles and an increasing cohesion.

A gradient-enhanced version of the theory [21] is employed. The formulation of gradient plasticity is based on [16, 8] and the present paper is a continuation of [22]. The enhancement was originally proposed in order to avoid the above-mentioned ill-posedness and mesh sensitivity problems in simulations of softening materials. Here, it is applied to hardening models which exhibit a softening response due to localization induced solely by non-associativity.

Another issue brought up in the paper is whether shear band instability can be simulated for contractant plasticity, since there is experimental evidence of such phenomena [12] and a negative dilatancy angle is attributed for instance to loose sands exhibiting liquefaction [33]. In fact, the gradient plasticity theory was previously used in [30, 31] to analyze analytically shear banding and pattern formation leading to liquefaction.

In Section 2 we recapitulate the classical and gradient-dependent Drucker–Prager plasticity theory. In Section 3 an analytical examination of the instability and localization in the theories is presented. In particular we consider the bifurcation properties via the acoustic tensor analysis according to [34] and discuss the properties of the gradient-dependent plasticity model. Section 4 contains numerous results of numerical simulations of the shear band formation in the biaxial (plane strain) compression test [37, 12]. Final remarks are gathered in Section 5.

In the paper we limit interest to quasi-static loading and small strains, so that the equilibrium and kinematic equations in the considered boundary value problem have the form

$$\mathbf{L}^{\mathrm{T}}\boldsymbol{\sigma} + \mathbf{b} = \mathbf{0}, \tag{1}$$

$$\boldsymbol{\epsilon} = \mathbf{L}\mathbf{u}, \tag{2}$$

where $\mathbf{L}$ is a differential operator matrix, $\boldsymbol{\sigma}$ is the stress tensor in a vector form, $\mathbf{b}$ is the body force vector, $\boldsymbol{\epsilon}$ is the strain tensor in a vector form, $\mathbf{u}$ is the displacement vector and the superscript T is the transpose symbol. The stresses and displacements satisfy the relevant natural and essential boundary conditions, respectively.

2. Drucker–Prager plasticity theory

According to experimental results, constitutive relations for geomaterials are pressure-sensitive and, furthermore, the direction of plastic flow is not normal with respect to the yield surface. Therefore, the behaviour of geomaterials must be described using a non-associated flow rule, which leads to a non-symmetry of the tangent stiffness operator. We focus attention on the Drucker–Prager plastic flow theory which incorporates a dilatant/contractant deformation and non-associativity. A gradient enhancement of the classical Drucker–Prager plasticity theory is used to preserve well-posedness of the governing equations and to analyze the whole deformation history. The equations for the classical and gradient-dependent Drucker–Prager plasticity are recollected below.

2.1. Classical Drucker–Prager plasticity

The classical Drucker–Prager yield function can be written as follows,

$$F(\boldsymbol{\sigma}, \kappa) = q + \alpha p - \beta c(\kappa)\,, \tag{3}$$

where $q = \sqrt{3J_2}$ and J_2 is the second invariant of the deviatoric stress tensor, $p = \frac{1}{3}(\sigma_{xx} + \sigma_{yy} + \sigma_{zz})$ is the hydrostatic pressure, α and β are functions of the internal friction angle φ:

$$\alpha = \frac{6\sin\varphi}{3 - \sin\varphi}\,, \qquad \beta = \frac{6\cos\varphi}{3 - \sin\varphi}\,, \tag{4}$$

c is a measure for the cohesion and κ is an invariant plastic strain measure (hardening parameter). The yield function satisfies the Kuhn–Tucker conditions,

$$\dot{\lambda} \geq 0\,, \qquad F \leq 0\,, \qquad \dot{\lambda} F = 0\,, \tag{5}$$

in which $\dot{\lambda}$ is a plastic multiplier. The multiplier determines the magnitude of the rate of plastic strains,

$$\dot{\boldsymbol{\epsilon}}^{\mathrm{p}} = \dot{\lambda}\mathbf{m}\,, \tag{6}$$

$\mathbf{m}$ is the plastic flow direction vector defined as the gradient of a plastic potential G,

$$\mathbf{m} = \frac{\partial G}{\partial \boldsymbol{\sigma}}\,, \qquad G = q + \overline{\alpha} p\,, \tag{7}$$

where $\overline{\alpha}$ is a function of the dilatancy angle ψ, similar to the definition of α in Eq. (4):

$$\overline{\alpha} = \frac{6\sin\psi}{3 - \sin\psi}\,. \tag{8}$$

The plastic consistency condition $\dot{F} = 0$ has the form

$$\frac{\partial F}{\partial \boldsymbol{\sigma}}\dot{\boldsymbol{\sigma}} + \frac{\partial F}{\partial \kappa}\dot{\kappa} = 0\,. \tag{9}$$

We introduce the gradient of the yield function $\mathbf{n}$,

$$\mathbf{n}^{\mathrm{T}} = \frac{\partial F}{\partial \boldsymbol{\sigma}}\,, \tag{10}$$

and the hardening modulus h

$$h(\kappa) = -\frac{\dot{\kappa}}{\dot{\lambda}}\frac{\partial F}{\partial \kappa}\,, \tag{11}$$

so that we can rewrite Eq. (9) in the form

$$\mathbf{n}^{\mathrm{T}}\dot{\boldsymbol{\sigma}} - h\dot{\lambda} = 0\,. \tag{12}$$

The stress rate $\dot{\boldsymbol{\sigma}}$ is derived from the constitutive relation

$$\dot{\boldsymbol{\sigma}} = \mathbf{D}^{\mathrm{e}}\left(\dot{\boldsymbol{\epsilon}} - \dot{\lambda}\mathbf{m}\right)\,, \tag{13}$$

in which $\mathbf{D}^{\mathrm{e}}$ is the elastic stiffness matrix. Equation (12) can be used to determine the plastic multiplier $\dot{\lambda}$ and the classical elastic-plastic tangent stiffness operator,

$$\mathbf{D}^{\mathrm{ep}} = \mathbf{D}^{\mathrm{e}} - \frac{\mathbf{D}^{\mathrm{e}}\mathbf{m}\mathbf{n}^{\mathrm{T}}\mathbf{D}^{\mathrm{e}}}{h + \mathbf{n}^{\mathrm{T}}\mathbf{D}^{\mathrm{e}}\mathbf{m}}\,. \tag{14}$$

To determine the relation between $\dot{\kappa}$ and $\dot{\lambda}$, the strain-hardening hypothesis is used leading to

$$\dot{\kappa} = \eta\dot{\lambda}, \qquad \eta = \left(1 + \frac{2}{9}\overline{\alpha}^2\right)^{\frac{1}{2}}\,, \tag{15}$$

so that proportionality of the plastic strain measure κ and the plastic multiplier λ is obtained. Using Eqs. (3) and (15) the hardening modulus reads

$$h(\kappa) = \eta\beta\frac{\partial c}{\partial \kappa}\,. \tag{16}$$

It is noted that both the friction and dilatancy angles are assumed to be constant due to two reasons: physically, the mobilized angles are asymptotic functions which attain their maximum value already for small deformations; algorithmically, the dependence of φ (or ψ) on for instance the equivalent plastic strain measure would disrupt the gradient plasticity formulation summarized in the next section.

2.2. Gradient-dependent Drucker–Prager plasticity

In the case of gradient-dependent Drucker–Prager plasticity, the yield function is additionally dependent on the Laplacian of the plastic strain measure κ. Assuming that only the cohesion exhibits the gradient dependence, the yield function takes the form

$$F(\boldsymbol{\sigma}, \kappa, \nabla^2\kappa) = q + \alpha p - \beta c(\kappa, \nabla^2\kappa) \,, \tag{17}$$

and the plastic potential function does not change.

The yield function satisfies the Kuhn–Tucker conditions (5). The gradient-dependence of the yield function implies that the plastic consistency condition $\dot{F} = 0$ is the following partial differential equation,

$$\frac{\partial F}{\partial \boldsymbol{\sigma}}\dot{\boldsymbol{\sigma}} + \frac{\partial F}{\partial \kappa}\dot{\kappa} + \frac{\partial F}{\partial \nabla^2\kappa}\nabla^2\dot{\kappa} = 0 \,. \tag{18}$$

The hardening modulus h is still defined by Eq. (16). If we introduce an additional variable g,

$$g(\kappa) = \frac{\dot{\kappa}}{\dot{\lambda}}\frac{\partial F}{\partial \nabla^2\kappa} = -\eta\beta\frac{\partial c}{\partial \nabla^2\kappa} \,, \tag{19}$$

the consistency condition (18) can be rewritten as:

$$\mathbf{n}^{\mathrm{T}}\dot{\boldsymbol{\sigma}} - h\dot{\lambda} + g\nabla^2\dot{\lambda} = 0 \,. \tag{20}$$

Note that for $g = 0$ the classical plastic flow theory is retrieved, but for $g \neq 0$ the plastic multiplier is a solution of the partial differential equation (20). In this paper the coefficient g is assumed to be constant for simplicity.

The finite element implementation is based on the following two weak-form equations governing the static equilibrium and the plastic consistency, respectively,

$$\int_V (\mathbf{L}\mathbf{v})^{\mathrm{T}}\boldsymbol{\sigma}\,\mathrm{d}V = \int_V \mathbf{v}^{\mathrm{T}}\mathbf{b}\,\mathrm{d}V + \int_S \mathbf{v}^{\mathrm{T}}\mathbf{t}\,\mathrm{d}S, \tag{21a}$$

$$\int_V wF\left(\boldsymbol{\sigma}, \kappa, \nabla^2\kappa\right)\mathrm{d}V = 0 \,, \tag{21b}$$

where $\mathbf{v}$ and w are suitable weighting functions, $\mathbf{t}$ is the traction vector. The integral in Eq. (21b) should formally be computed over the volume of the plastic part of the body, but it is assumed that in the elastic part the value of the yield function will be set to zero while performing this integration.

Equations (21) are written for iteration $i+1$ of the incremental-iterative algorithm and the following decomposition is used,

$$\boldsymbol{\sigma}^{(i+1)} = \boldsymbol{\sigma}^{(i)} + \mathrm{d}\boldsymbol{\sigma} \,, \qquad \lambda^{(i+1)} = \lambda^{(i)} + \mathrm{d}\lambda, \tag{22}$$

so that the yield function F can be developed in a truncated Taylor series around $(\boldsymbol{\sigma}^{(i)}, \lambda^{(i)})$. We obtain the following incremental equations,

$$\int_V (\mathbf{L}\mathbf{v})^{\mathrm{T}}\mathrm{d}\boldsymbol{\sigma}\,\mathrm{d}V = f_{\mathrm{ext}} - f_{\mathrm{int}}, \tag{23a}$$

$$\int_V w\left[\mathbf{n}^{\mathrm{T}}\mathrm{d}\boldsymbol{\sigma} - h\,\mathrm{d}\lambda + g\nabla^2(\mathrm{d}\lambda)\right]\mathrm{d}V = -\int_V wF\left(\boldsymbol{\sigma}^{(i)}, \kappa^{(i)}, \nabla^2\kappa^{(i)}\right)\mathrm{d}V, \tag{23b}$$

with

$$f_{\mathrm{ext}} = \int_S \mathbf{v}^{\mathrm{T}}\mathbf{t}\,\mathrm{d}S + \int_V \mathbf{v}^{\mathrm{T}}\mathbf{b}\,\mathrm{d}V, \tag{24a}$$

$$f_{\mathrm{int}} = \int_V (\mathbf{L}\mathbf{v})^{\mathrm{T}}\boldsymbol{\sigma}^{(i)}\,\mathrm{d}V. \tag{24b}$$

Next, we substitute the incremental form of Eq. (13) into Eqs. (23) to obtain

$$\int_V (\mathbf{Lv})^{\mathrm{T}}(\mathbf{D}^{\mathrm{e}}\mathrm{d}\boldsymbol{\epsilon})\,\mathrm{d}V - \int_V (\mathbf{Lv})^{\mathrm{T}}(\mathbf{D}^{\mathrm{e}}\mathbf{m}\,\mathrm{d}\lambda)\,\mathrm{d}V = f_{\mathrm{ext}} - f_{\mathrm{int}}, \tag{25a}$$

$$\int_V w\mathbf{n}^{\mathrm{T}}\mathbf{D}^{\mathrm{e}}\mathrm{d}\boldsymbol{\epsilon}\,\mathrm{d}V - \int_V w\left[(h+\mathbf{n}^{\mathrm{T}}\mathbf{D}^{\mathrm{e}}\mathbf{m})\mathrm{d}\lambda + g\nabla^2(\mathrm{d}\lambda)\right]\mathrm{d}V = -\int_V wF\left(\boldsymbol{\sigma}^{(i)}, \kappa^{(i)}, \nabla^2\kappa^{(i)}\right)\mathrm{d}V. \tag{25b}$$

Now, the plastic multiplier field is discretized next to the classical discretization of the displacements. It is important to notice that, if the yield condition (17) is used in the classical return mapping algorithm to distinguish between elastic and plastic states, a C^1-continuous interpolation of λ is unavoidable, otherwise $\nabla^2\lambda$ loses meaning [21]. Therefore, the Laplacian term is not removed from the left-hand side of Eq. (23b), although this can be done using Green's formula if a homogeneous non-standard boundary condition $(\nabla\mathrm{d}\lambda)^{\mathrm{T}}\boldsymbol{\nu} = 0$ is assumed ($\boldsymbol{\nu}$ is a vector normal to the surface of the plastic part of the body). Further details of the finite element implementation can be found in [21, 9].

3. Instability indicators

3.1. Material instability and loss of ellipticity

According to the classical definition of material stability [13, 15] a material is stable if its constitutive relationship satisfies the condition of a positive second order work density,

$$\dot{\epsilon}_{ij}\dot{\sigma}_{ij} > 0\,, \tag{26}$$

where $\dot{\epsilon}_{ij}$ and $\dot{\sigma}_{ij}$ are the strain and stress rate tensors, respectively, and the summation convention is adopted. We limit our consideration to incrementally linear constitutive equations,

$$\dot{\sigma}_{ij} = D_{ijkl}\dot{\epsilon}_{kl}\,. \tag{27}$$

Then, a material instability is indicated by the loss of positive-definiteness of the tangent stiffness tensor D_{ijkl}, i.e. by the singularity of the symmetric part of D_{ijkl},

$$\det(D_{ijkl} + D_{klij}) = 0\,. \tag{28}$$

Since it can be shown [36] that the smallest eigenvalue of D_{ijkl} is larger than or equal to the smallest eigenvalue of its symmetric part, for a non-symmetric tangent stiffness tensor the loss of material stability may occur in the deformation history prior to the limit point and loss of uniqueness related to a diffuse bifurcation, cf. [35, 10], which are marked by the condition

$$\det(D_{ijkl}) = 0\,. \tag{29}$$

As shown in [36], the special structure of the elastic-plastic tangent operator $\mathbf{D}^{\mathrm{ep}}$ in Eq. (14) implies that it has only real eigenvalues even if it is non-symmetric, so that condition (29) is satisfied only when $h = 0$. This means that if we assume $h > 0$ the diffuse bifurcation will never occur.

However, when the material stability has been lost, a so-called discontinuous bifurcation is also possible, cf. [24, 19, 36, 20, 10]. For a homogeneous and homogeneously deformed body we investigate the possibility that upon a further increment of deformation a discontinuity of the deformation gradient across a plane with normal ν_i is admitted,

$$[\![\, u_{i,j} \,]\!] \neq 0, \tag{30}$$

where $[\![\ ]\!]$ denotes a jump of a quantity. During this bifurcation the continuity of displacements and the equilibrium condition are preserved pointwise. If the deformation satisfies the kinematic

compatibility equations, it must be piecewise homogeneous, so that, for an arbitrary vector μ_i, the strain jump has the form

$$[\![\epsilon_{ij}]\!] = \frac{1}{2}(\nu_i \mu_j + \nu_j \mu_i) \,. \tag{31}$$

With the piecewise linear constitutive equation (27) we obtain the stress rate jump at the onset of the discontinuity,

$$[\![\dot{\sigma}_{ij}]\!] = D_{ijkl} [\![\dot{\epsilon}_{kl}]\!] \,, \tag{32}$$

where it has been assumed that the same tangent stiffness moduli govern the material behaviour on both sides of the discontinuity plane (cf. the concept of a linear comparison solid [13]). Equilibrium requires that during the formation of the discontinuity the tractions t_j are continuous across the plane with normal ν_i,

$$[\![\dot{t}_j]\!] = \nu_i [\![\dot{\sigma}_{ij}]\!] = 0, \tag{33}$$

so substituting Eq. (32) and the rate form of Eq. (31), and exploiting the (minor) symmetry property $D_{ijkl} = D_{ijlk}$ we obtain the equation

$$(\nu_i D_{ijkl} \nu_l)\, \mu_k = 0, \tag{34}$$

which has a non-trivial solution only when the determinant of the so-called acoustic tensor $Q_{jk} = \nu_i D_{ijkl} \nu_l$ vanishes,

$$\det(Q_{jk}) = 0. \tag{35}$$

For a given tangent stiffness the last condition yields a vector ν_l, which defines the discontinuity direction, the vector μ_k can then be determined from Eq. (34) and the jump mode $\nu_l \mu_k$ is known. For a shear band the vector ν_l is perpendicular to μ_k.

The singularity of the acoustic tensor and the formation of the discontinuity correspond to the local loss of ellipticity of the rate equilibrium equations. Ellipticity is one of the necessary conditions for well-posedness of the rate boundary value problem, cf. [10]. Here, well-posedness is understood as the existence of a finite number of linearly independent and continuous solutions.

The emergence of the discontinuities in the deformation gradient has traditionally been identified with strain localization [24]. A shear band may then be viewed as a zone of intense deformation bounded by two discontinuity planes. However, since the distance between those planes remains undefined for a classical material model, they coincide giving localization in a set of measure zero. In this paper the notion of strain localization is understood in a broader sense, as the emergence of bands of concentrated deformation due to material instabilities. Nevertheless, the first point in the deformation history for which there exists a nontrivial solution of Eq. (34) marks the possible onset of localization.

3.2. Properties of the gradient model

The enhancement of the classical theory was made in order to preserve well-posedness of the governing equations for the case when a softening relation between stresses and strains is assumed ($h < 0$). For a softening medium the factor g can be associated with an internal length parameter l, for instance in a one-dimensional analytical solution we have $g = -hl^2 > 0$ [8, 22]. However, also for a hardening material the Laplacian term with $g > 0$ regularizes the solution in the sense that a higher-order continuity of the strain field is obtained [9]. In this paper the gradient enhancement is applied to Drucker–Prager non-associative materials with constant friction and dilatancy angles and a non-softening cohesion. The non-symmetry of the constitutive operator induces the material instability and shear band localization and the effectiveness of a gradient enhancement of the cohesion is verified.

To analyze the possible influences of the gradient term on the material stability and ellipticity of the governing equations, we first consider a uniaxial case of a shear layer with length L. The consistency condition (20) then gives

$$\dot{\tau} = h\dot{\gamma}^{\mathrm{p}} - g\dot{\gamma}^{\mathrm{p}}_{xx}, \tag{36}$$

with $\dot{\gamma}^{\mathrm{p}} = \dot{\lambda}$. We calculate the second order work according to the material stability condition (26). The destabilizing effect of softening is introduced only by the plastic action and the work corresponding to the plastic strain $\dot{\gamma}^{\mathrm{p}}$ equals

$$\int_{-L/2}^{L/2} \dot{\tau}\dot{\gamma}^{\mathrm{p}}\,\mathrm{d}x = \int_{-w/2}^{w/2} [h(\dot{\gamma}^{\mathrm{p}})^2 - g\dot{\gamma}^{\mathrm{p}}_{xx}\dot{\gamma}^{\mathrm{p}}]\,\mathrm{d}x = \int_{-w/2}^{w/2} h(\dot{\gamma}^{\mathrm{p}})^2\,\mathrm{d}x + \int_{-w/2}^{w/2} g(\dot{\gamma}^{\mathrm{p}}_{x})^2\,\mathrm{d}x, \tag{37}$$

where w is the width of the plastic zone and the boundary condition $\dot{\gamma}^{\mathrm{p}} = 0$ for $x \pm w/2$ has been used. We observe that for $h < 0$ the first term in Eq. (37) introduces instability, while the second (gradient) term acts as a stabilizer. On the other hand, if we adopted $g = -hl^2$ for $h > 0$ (hardening) the gradient term would act in a destabilizing manner. Therefore, the gradient coefficient g is assumed to be positive irrespective of the sign of h.

Next, we calculate $\dot{\lambda}$ from Eq. (20) and substitute into the constitutive relation (13) to obtain after regrouping

$$\dot{\boldsymbol{\epsilon}} - \frac{g}{h}\nabla^2\dot{\lambda}\mathbf{m} = \left[(\mathbf{D}^{\mathrm{e}})^{-1} + \frac{1}{h}\mathbf{m}\mathbf{n}^{\mathrm{T}}\right]\dot{\boldsymbol{\sigma}}, \tag{38}$$

so that with the aid of the Sherman–Morrison formula the gradient-dependent elastic-plastic stress–strain relation can be written in the tensor form as

$$\dot{\sigma}_{ij} = D_{ijkl}\dot{\epsilon}_{kl} + g_{ij}\nabla^2\dot{\lambda}, \tag{39}$$

with the standard elastic-plastic tangent stiffness tensor D_{ijkl} defined in a matrix form in Eq. (14) and the tensor g_{ij} as follows,

$$g_{ij} = -g\,\frac{D_{ijkl}m_{kl}}{h + n_{ij}D_{ijkl}m_{kl}}\,. \tag{40}$$

In analogy to the above ellipticity analysis we can consider the possibility of emergence of a discontinuity across a plane with a normal ν_i, which in addition to a jump in the deformation gradient involves a jump in the second order gradient of the equivalent plastic strain, cf. [35]. The first jump can be represented as in Eq. (31) and the second can be written as follows,

$$[\![\, \nabla^2\dot{\lambda} \,]\!] = \nu_k\alpha_k\,, \tag{41}$$

with an arbitrary vector α_k. Using the equilibrium condition (33) and the constitutive relation (39) we can write

$$[\![\, \dot{t}_j \,]\!] = \nu_i[\![\, \dot{\sigma}_{ij} \,]\!] = (\nu_i D_{ijkl}\nu_l)\,\mu_k + (\nu_i g_{ij}\nu_k)\,\alpha_k = 0. \tag{42}$$

The occurrence of the discontinuity plane is only possible if, for arbitrary μ_k and α_k, both contributions in Eq. (42) vanish simultaneously. This does not happen except possibly for some special structure of the constitutive operator. Since violation of the bifurcation condition as defined by Eqs. (30) and (33) guarantees ellipticity, we conclude that the gradient-dependence has a regularizing effect. Consequently the rate boundary value problem for a gradient-dependent elastic-plastic continuum remains well-posed in the unstable regime and localization in a set of measure zero is prevented.

It is noted that for the gradient dependent continuum the critical value of the hardening modulus and the direction of the localization band can be determined from the classical condition of the

acoustic tensor singularity (35), since prior to the moment of bifurcation into a localized deformation pattern the gradient terms have no influence on the solution.

Therefore, before we embark on the nonlinear instability analysis with the gradient-enhanced model, an analytical examination of the acoustic tensor is performed. The analysis is based on the algorithm described in [34], which determines the normalized value of the determinant of the acoustic tensor as a function of an angle defining the direction of the discontinuity plane in a two-dimensional case.

3.3. Analysis of acoustic tensor properties

The analysis of the acoustic tensor properties is performed in order to indicate the loss of ellipticity for the non-associated Drucker–Prager model with a non-negative hardening modulus and to find out which factors influence it. Calculations are carried out for the case of plane strain biaxial compression (see a typical configuration in Fig. 1) and, with the exception of one case, the onset of plastic yielding is considered. In further considerations we adopt for conciseness the following notation: $a = \sin\varphi$, $b = \sin\psi$, $h_c = \frac{\partial c}{\partial \kappa}$.

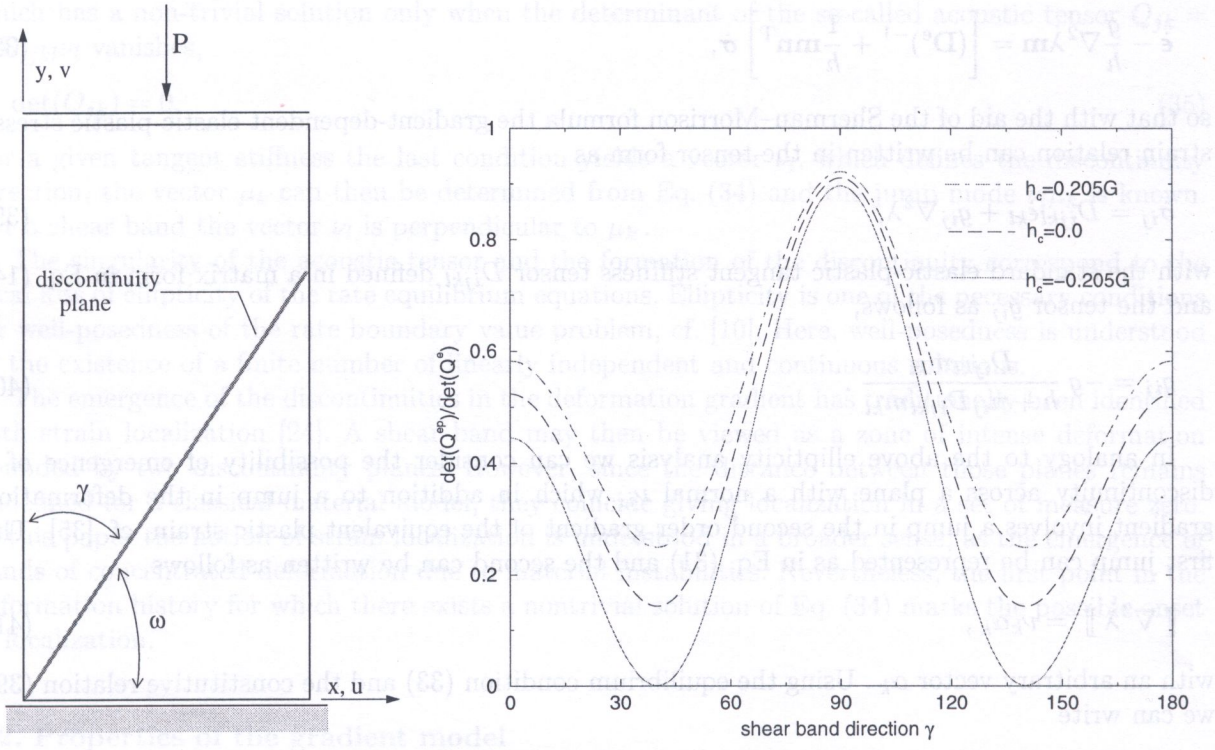

Fig. 1. The sample and the influence of h_c on the determinant of the acoustic tensor

The first computations are performed to analyze the influence of inclination of cohesion hardening diagram h_c on the results. The following data are adopted: Young's modulus $E = 2400\ \frac{\mathrm{N}}{\mathrm{mm}^2}$, Poisson's ratio $\nu = 0.2$, $\sin\varphi = 0.5$, $\sin\psi = 0.0$. The purpose is to find the value of h_c for which elastic-plastic localization tensor $\mathbf{Q}^{\mathrm{ep}}$ exhibits a singularity. As can be read from Fig. 1, for the given data a discontinuous bifurcation is possible only for cohesion softening. The maximum value of h_c for which $\det(\mathbf{Q}^{\mathrm{ep}}) = 0$ is equal to approximately -0.205 of shear modulus G and the corresponding discontinuity direction estimated from the diagram is $\gamma \approx 40°$, where γ is an angle between the axis of the minimum (compressive) principal stress $\sigma_y = \sigma_2$ and the discontinuity direction.

Then, we investigate the influence of the internal friction angle φ and the dilatancy angle ψ on the possibility of the discontinuous bifurcation. In all simulations we assume that $\varphi > \psi$ since it has been proven for cohesionless soils that this assumption is necessary to ensure that the amount of dissipated energy is non-negative [33]. The first analysis is done for a constant difference between $a = \sin\varphi$ and $b = \sin\psi$ equal to 0.5 (Fig. 2). The second example is computed for $\sin\varphi = 0.5$ and a varying value of $\sin\psi$ (Fig. 2). Figure 3 depicts the results for $\sin\psi = 0.0$ and a series of values of $\sin\varphi$ both at the onset of plastic yielding ($\frac{\sigma_3}{\sigma_2} = \nu$) and at the limit point ($\frac{\sigma_3}{\sigma_2} \to 0.5$), with data taken from the output of a one element test. As expected, the analysis of the diagrams indicates that instability increases with a decreasing value of $\sin\psi$ and with growing non-associativity. It is worth noting that in the case of contractant plasticity ($\psi < 0$), the material becomes very unstable and for certain data a discontinuous bifurcation is possible even at the onset of plasticity.

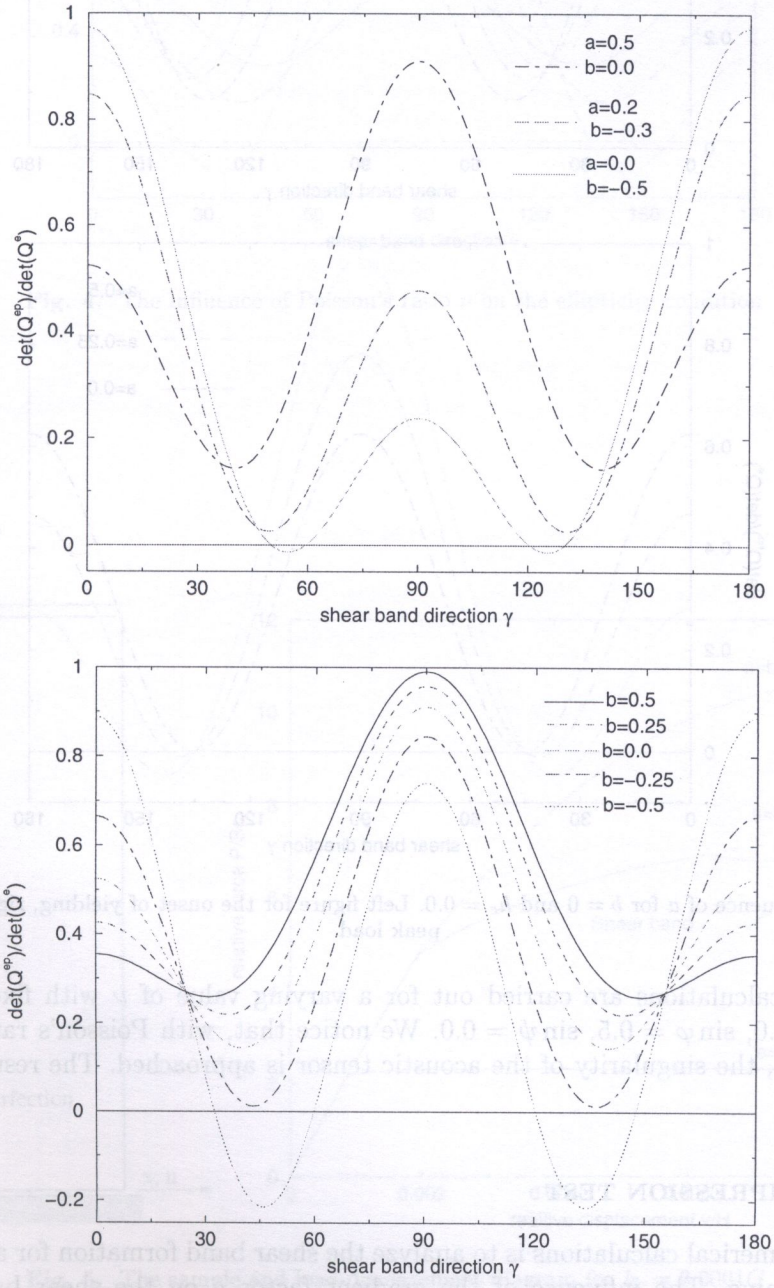

Fig. 2. The values of the normalized determinant of the acoustic tensor for $a - b = 0.5$ (left) and the influence of $b = \sin\psi$ for $a = \sin\varphi = 0.5$ (right); $h_c = 0.0$ in both cases

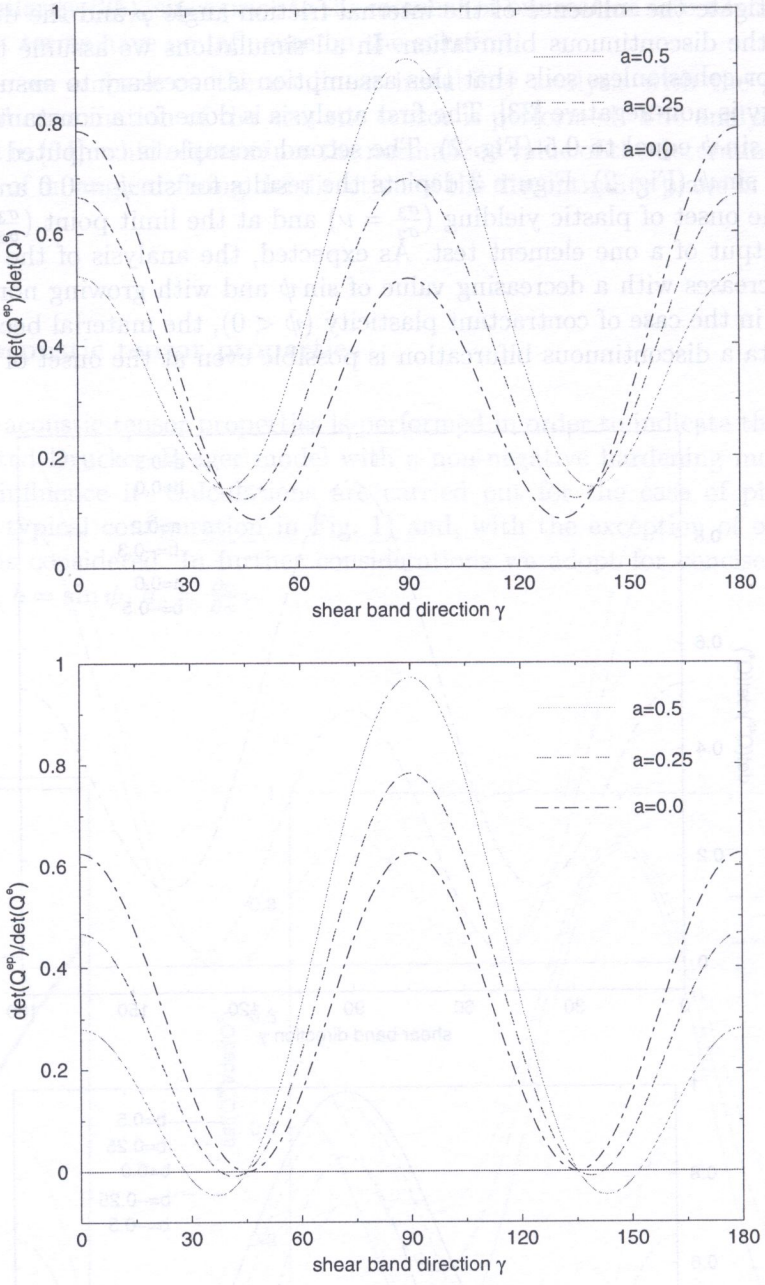

Fig. 3. The influence of a for $b = 0$ and $h_c = 0.0$. Left figure for the onset of yielding, right figure for the peak load

The following calculations are carried out for a varying value of ν with fixed values of $G = 1000\ \frac{\mathrm{N}}{\mathrm{mm}^2}$, $h_c = 0.0$, $\sin\varphi = 0.5$, $\sin\psi = 0.0$. We notice that, with Poisson's ratio growing to 0.5 (incompressibility), the singularity of the acoustic tensor is approached. The results are plotted in Fig. 4.

4. Biaxial compression test

The first aim of numerical calculations is to analyze the shear band formation for a varying intensity of cohesion hardening. The influence of the gradient factor g on the shear band width is also investigated. Another goal is to simulate localization for the case of contractant plasticity (negative value of $\sin\psi$). Eventually, a comparison of results for a coarse and fine mesh is done. We focus

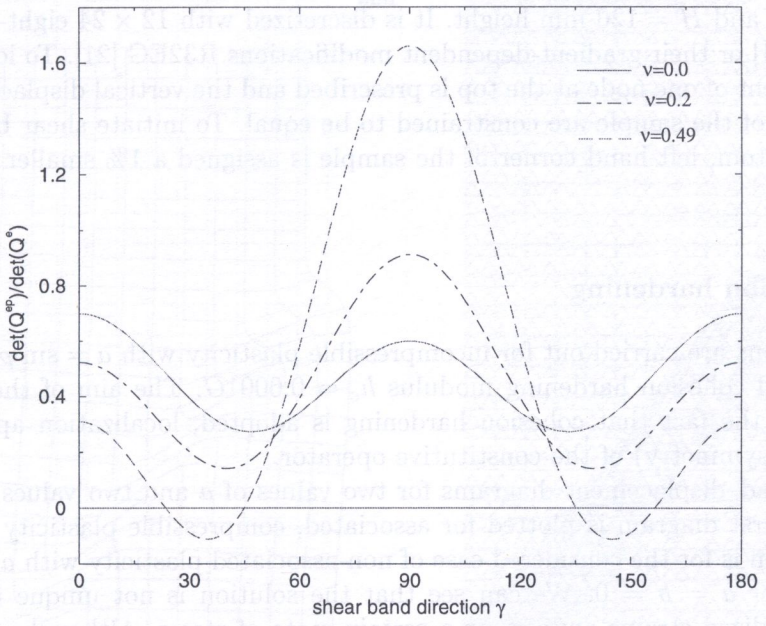

Fig. 4. The influence of Poisson's ratio ν on the ellipticity condition

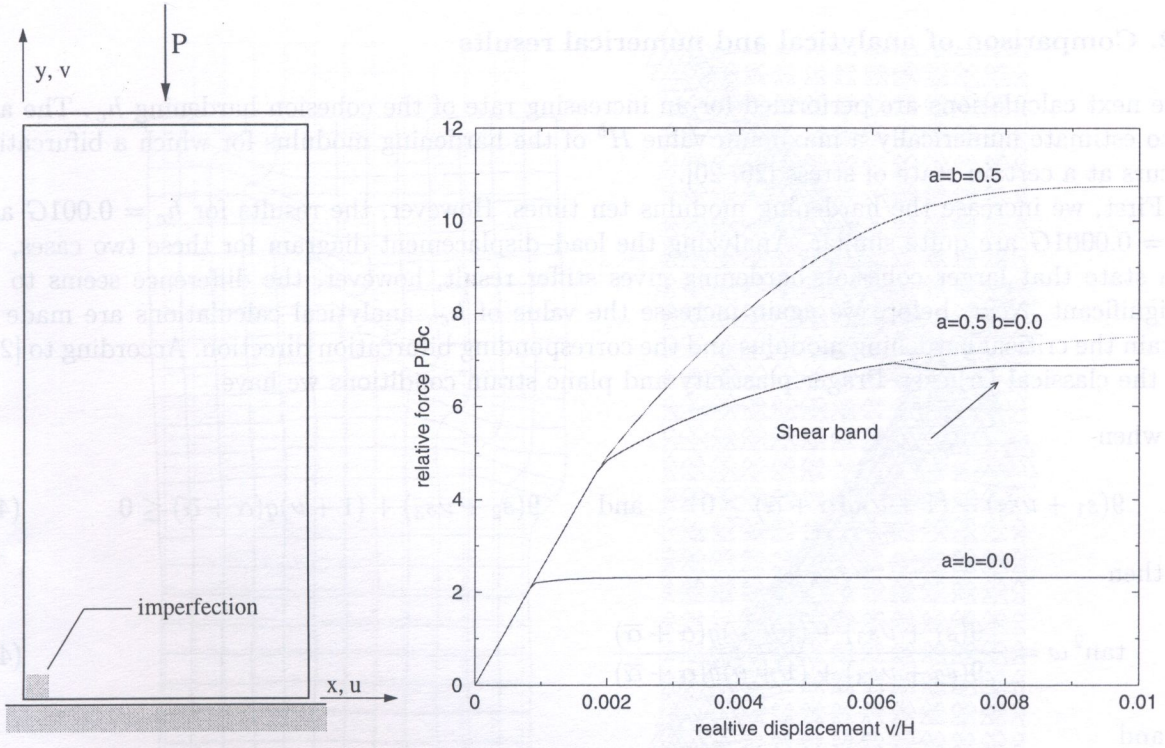

Fig. 5. The sample and load-displacement diagram for $h_c = 0.0001G$

our attention on a standard plane strain biaxial compression test [37, 12], shown in Fig. 5. The constant material data are as follows: $E = 2400\ \frac{\mathrm{N}}{\mathrm{mm}^2}$, $\nu = 0.2$. The dimensions of the specimen are: $B = 60$ mm width and $H = 120$ mm height. It is discretized with 12×24 eight-noded plane strain elements CQ16E [1] or their gradient-dependent modifications R32EG [21]. To load the sample, the vertical displacement of one node at the top is prescribed and the vertical displacements of all nodes at the upper edge of the sample are constrained to be equal. To initiate shear band formation one element in the bottom, left-hand corner of the sample is assigned a 1% smaller value of the initial cohesion.

4.1. Small cohesion hardening

The first calculations are carried out for incompressible plasticity with $a = \sin\varphi = 0.5$, $b = \sin\psi = 0.0$, $g = 0.1$ N and cohesion hardening modulus $h_c = 0.0001G$. The aim of the calculations is to show that despite the fact that cohesion hardening is adopted, localization appears due to non-associativity (non-symmetry) of the constitutive operator.

In Fig. 5 the load–displacement diagrams for two values of a and two values of b are shown for comparison. The first diagram is plotted for associated, compressible plasticity with $a = b = 0.5$. The second diagram is for the considered case of non-associated plasticity with $a = 0.5$ and $b = 0.0$, the third one is for $a = b = 0$. We can see that the solution is not unique in the second case and a band of localized strains appears at a certain state of stress. Although in general the local unstable behaviour can be stabilized by the surrounding material, in the considered test ellipticity is lost almost simultaneously in many points and a shear band develops. The analysis of localized deformation patterns and plastic strain distribution provides the information that the shear band evolves with the deformation level, i.e. it moves from the bottom towards the top of the sample. This will be shown in the next section.

4.2. Comparison of analytical and numerical results

The next calculations are performed for an increasing rate of the cohesion hardening h_c. The aim is to estimate numerically a maximum value H^b of the hardening modulus for which a bifurcation occurs at a certain state of stress [26, 20].

First, we increase the hardening modulus ten times. However, the results for $h_c = 0.001G$ and $h_c = 0.0001G$ are quite similar. Analyzing the load–displacement diagram for these two cases, we can state that larger cohesion hardening gives stiffer result, however, the difference seems to be insignificant. Next, before we again increase the value of h_c, analytical calculations are made to obtain the critical hardening modulus and the corresponding bifurcation direction. According to [26], for the classical Drucker–Prager plasticity and plane strain conditions we have:

when

$$9(s_1 + \nu s_3) + (1+\nu)q(\alpha + \overline{\alpha}) \geq 0 \qquad \text{and} \qquad 9(s_2 + \nu s_3) + (1+\nu)q(\alpha + \overline{\alpha}) \leq 0 \tag{43}$$

then

$$\tan^2\omega = -\frac{9(s_1 + \nu s_3) + (1+\nu)q(\alpha + \overline{\alpha})}{9(s_2 + \nu s_3) + (1+\nu)q(\alpha + \overline{\alpha})} \tag{44}$$

and

$$\frac{H^b}{2G} = \frac{1+\nu}{36(1-\nu)}\left[2(\alpha - \overline{\alpha})^2 - (1-\nu)\left(\frac{9s_3}{q} + \alpha + \overline{\alpha}\right)^2\right]. \tag{45}$$

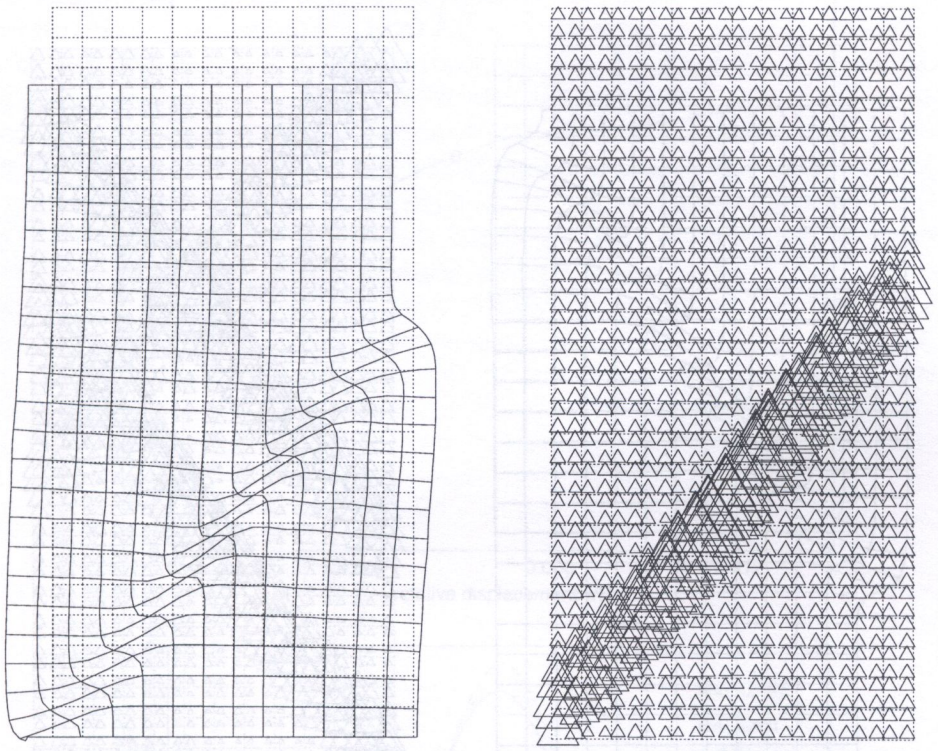

Fig. 6. Shear band formation and equivalent plastic strains for the upper edge displacement equal to 1.3 mm. Triangles in the figure illustrate equivalent plastic strain distribution, their sizes are proportional to the strain value

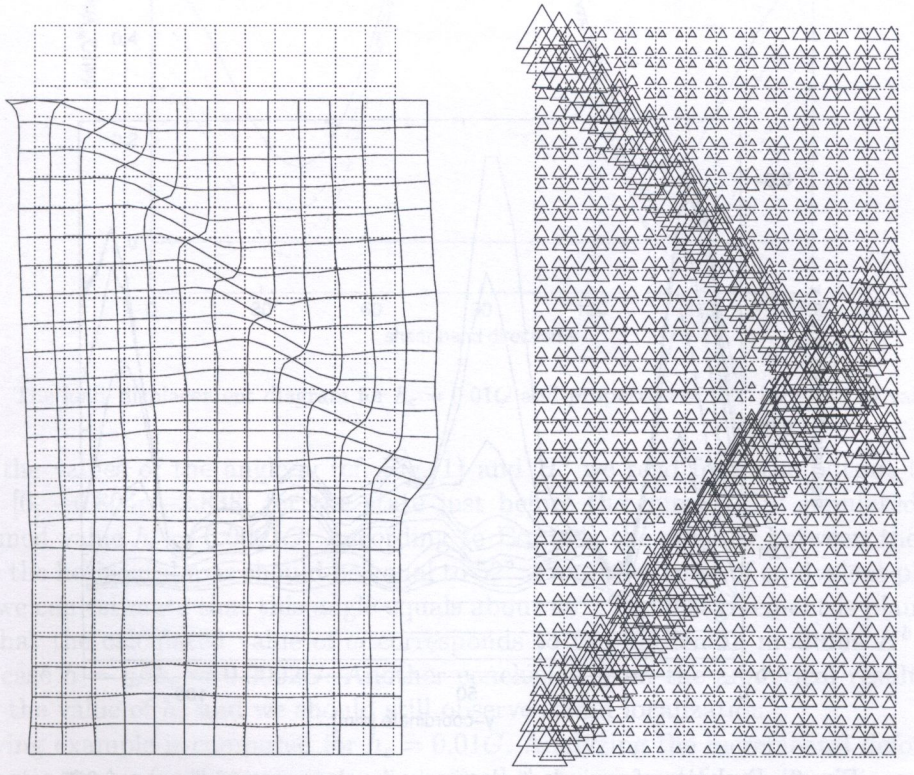

Fig. 7. Incremental displacement pattern and equivalent plastic strains for the upper edge displacement equal to 1.6 mm

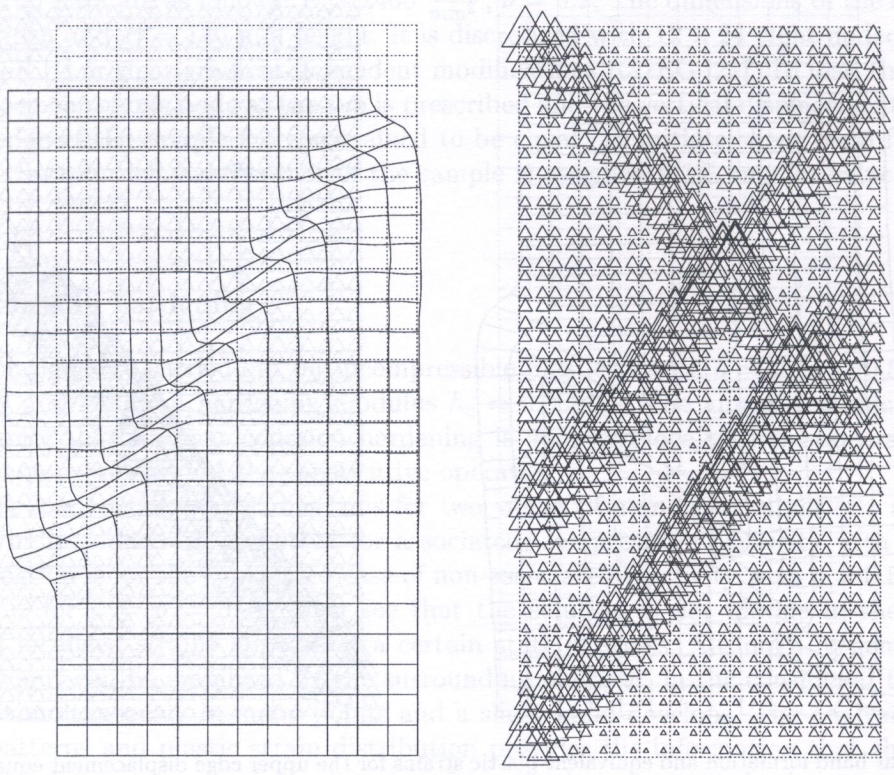

Fig. 8. Incremental displacement pattern and equivalent plastic strains for the upper edge displacement equal to 1.9 mm

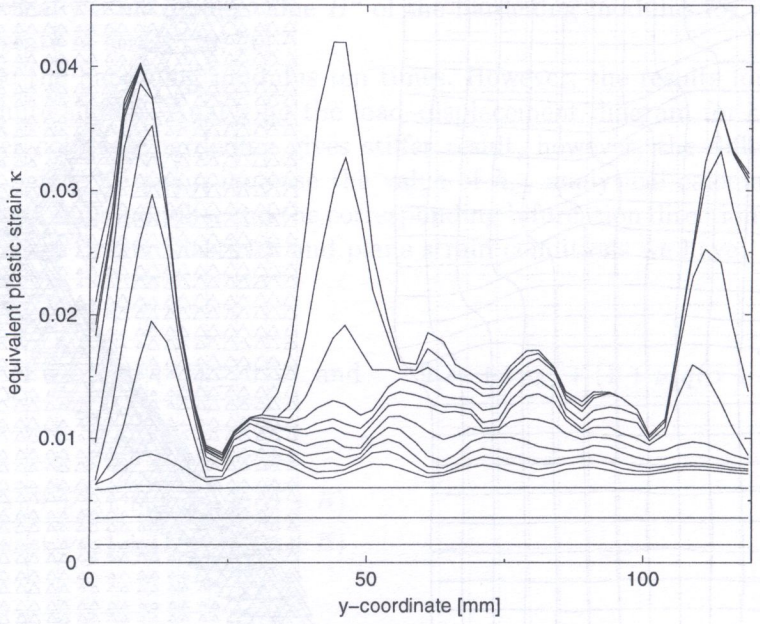

Fig. 9. Evolution of equivalent plastic strains along vertical line $x = 6.057$

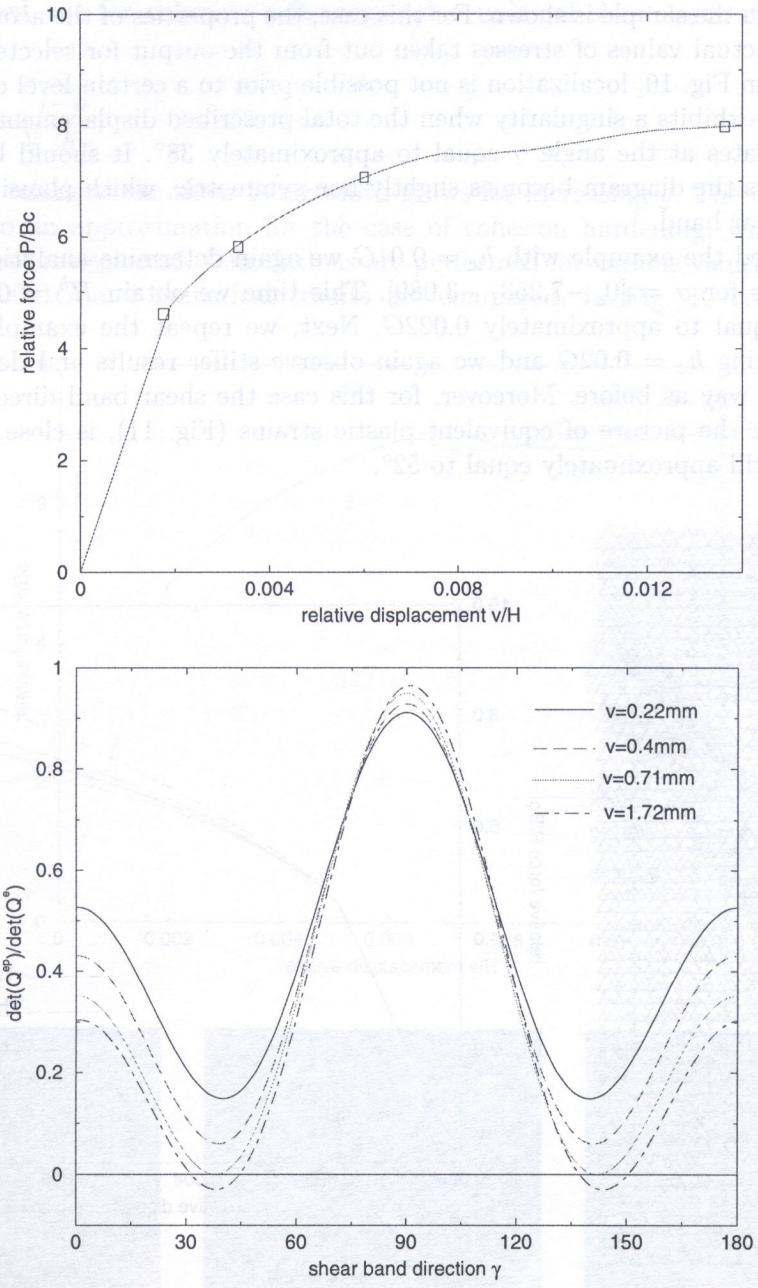

Fig. 10. The load–displacement diagram for $h_c = 0.01G$ and properties of $\mathbf{Q}^{ep}$ for selected values of v

To calculate the values of the angle ω (cf. Fig. 1) and H^b we read from the output the principal stresses $\sigma = [0, -6.804, -2.838]$ for the state just before the numerically simulated bifurcation and the assumed value $h_c = 0.0001G$. According to Eq. (44) the angle ω between the shear band direction and the horizontal axis should be equal to 52°. From the figure of equivalent plastic strains (not shown) we can estimate that this angle equals about 48°. The disagreement is plausibly caused by the fact that the calculated value of ω corresponds to the hardening modulus $H^b = 0.0308G$, while in our case $h = \eta\beta h_c \approx 0.0002G$. Another conclusion from the analytical results is that we may increase the value of h_c and we should still observe strain localization.

The following example is computed for $h_c = 0.01G$. Analyzing the incremental deformation and equivalent plastic strains for that case it can be noticed that various deformation patterns depending on the stage of loading are obtained. The history of shear band formation for an increasing level of deformation is shown in Figs. 6–8. In Fig. 9 the evolution of equivalent plastic strains along a

vertical line through the sample is shown. For this case, the properties of the acoustic tensor are also examined for the actual values of stresses taken out from the output for selected levels of loading. As can be read from Fig. 10, localization is not possible prior to a certain level of deformation. The localization tensor exhibits a singularity when the total prescribed displacement v equals 0.71 mm. A shear band initiates at the angle γ equal to approximately 38°. It should be noted that after localization appears the diagram becomes slightly non-symmetric, which plausibly happens due to presence of the shear band.

Having computed the example with $h_c = 0.01G$ we again determine analytically the maximum hardening modulus for $\sigma = [0, -7.253, -3.089]$. This time we obtain $H^b = 0.045G$, so that the maximum h_c is equal to approximately $0.022G$. Next, we repeat the example for a larger rate of cohesion hardening $h_c = 0.02G$ and we again observe stiffer results and deformation patterns evolve in a similar way as before. Moreover, for this case the shear band direction, which can be approximated from the picture of equivalent plastic strains (Fig. 11), is close to the analytically calculated value, still approximately equal to 52°.

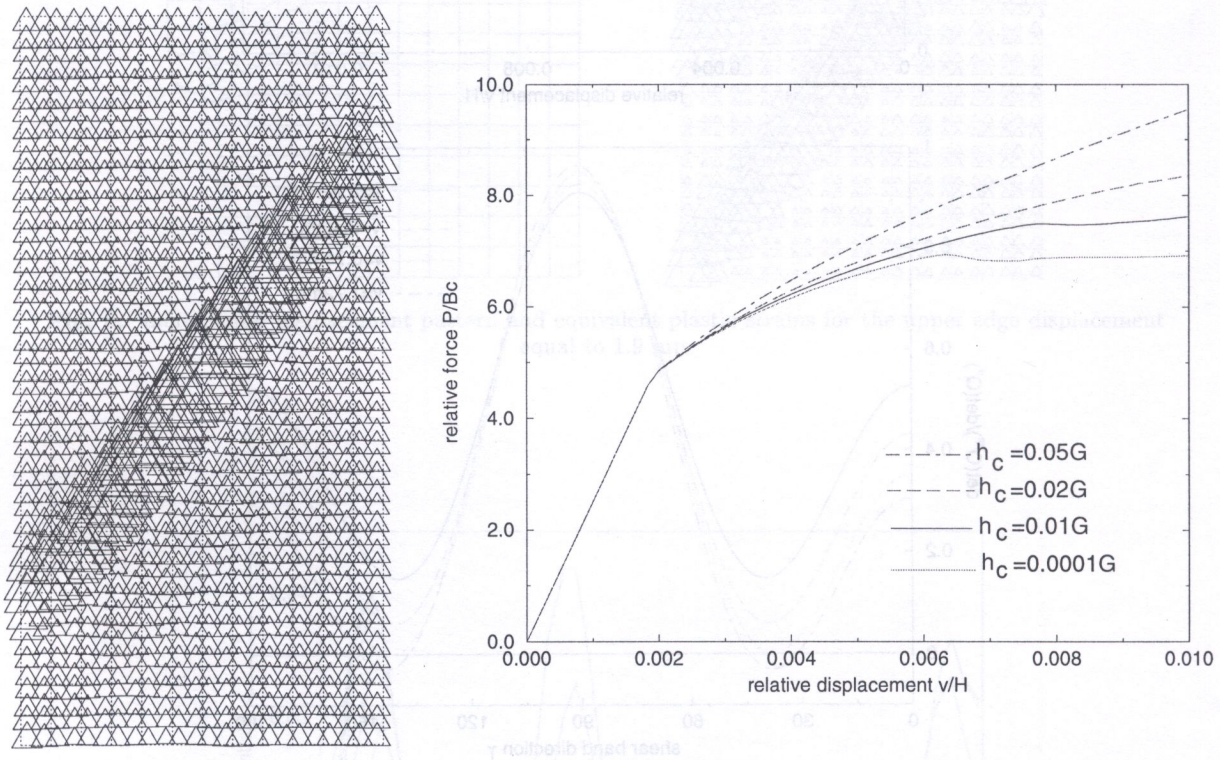

Fig. 11. Equivalent plastic strains for $h_c = 0.02G$ (left) and comparison of results for various values of h_c (right)

Taking the numerical and analytical results into account we can state that the critical value of the hardening modulus has almost been reached. Finally, to show that localization does not appear for $h > H^b$, the example with $h_c = 0.05G$ is calculated. This time we observe a homogeneous strain distribution.

The load–displacement diagrams for various values of h_c are shown in Fig. 11. It can be observed that the larger cohesion hardening is applied, the stiffer results we obtain.

4.3. Influence of g on shear band width

The second aim of our research is to evaluate the effect of the gradient scaling factor g on the results. Theoretical relations between g, h, l and w (where l – internal length scale and w – shear

band width), worked out for cohesion softening and a uniaxial shear layer case [22] are as follows,

$$w = 2\pi l, \qquad l = \sqrt{\frac{-g}{h}}. \tag{46}$$

According to these relations the shear band width grows for increasing g. The question is whether formula (46) is also an approximation for the case of cohesion hardening, when the minus sign under the square root is neglected. Calculations are performed for various values of g with $a = 0.5$, $b = 0.0$, $h_c = 0.0001G$ and numerical results are compared. In Fig. 12 contour plots of the

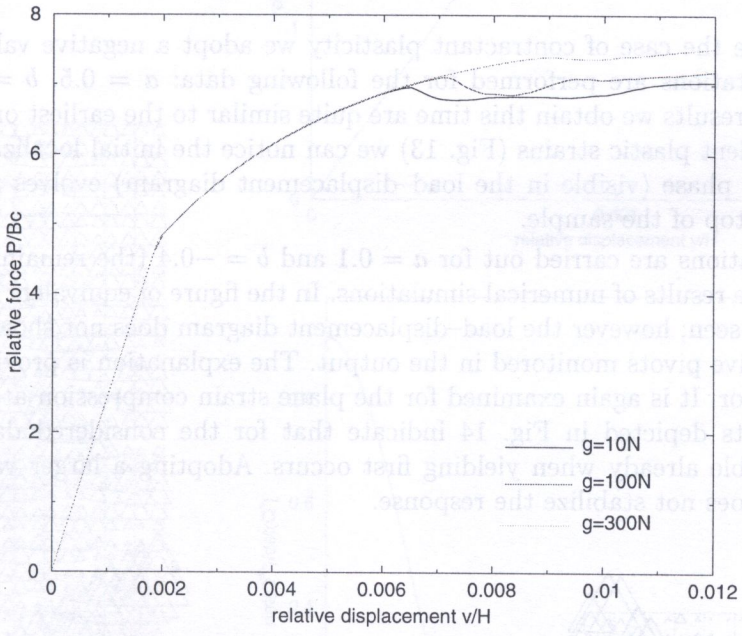

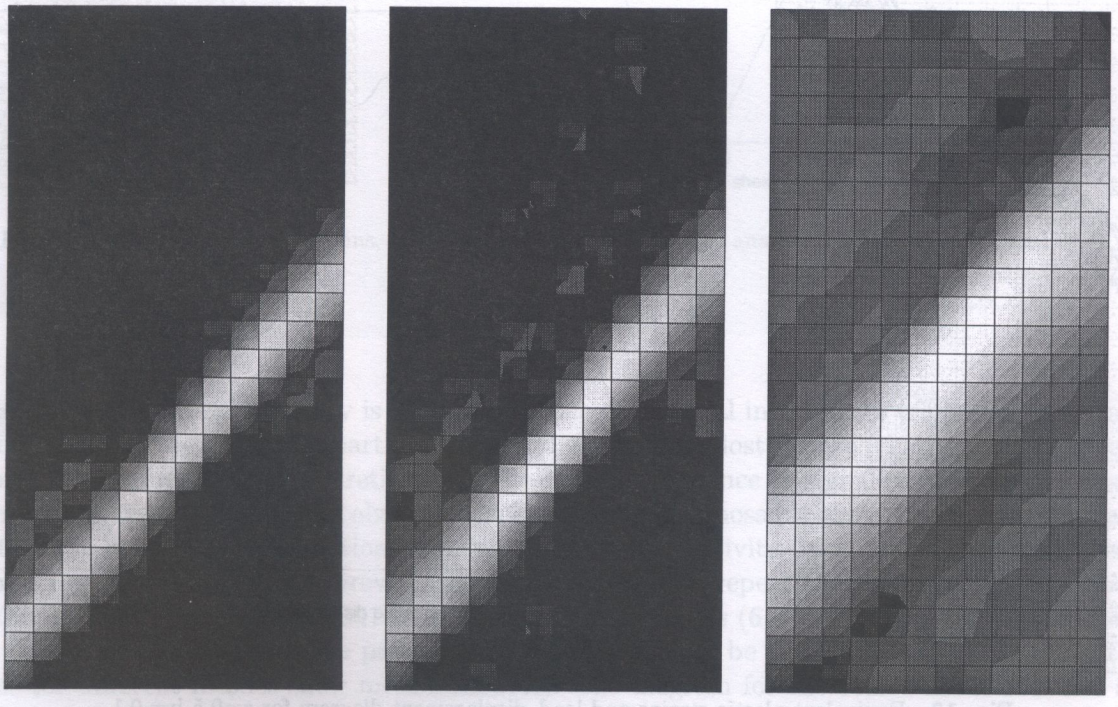

Fig. 12. Comparison of load–displacement diagrams and shear band widths for a growing value of gradient influence coefficient g

equivalent plastic strain for three values of g: 10 N, 100 N and 300 N are presented. We can state that in the case of cohesion hardening the shear band width still increases with growing g (stronger regularization effect), but the relations between g, l and h in Eq. (46) do not seem to hold. As expected, the load–displacement diagrams in Fig. 12 show that the response becomes stiffer with growing g, since the gradient term has a stabilizing effect on the solution.

4.4. Contractant plasticity

In order to simulate the case of contractant plasticity we adopt a negative value of the dilatancy angle. First computations are performed for the following data: $a = 0.5$, $b = -0.1$, $g = 0.1$ N, $h_c = 0.0001G$. The results we obtain this time are quite similar to the earliest ones (Section 4.2). In the figure of equivalent plastic strains (Fig. 13) we can notice the initial localization pattern which after a rehardening phase (visible in the load–displacement diagram) evolves and the shear band moves towards the top of the sample.

The next calculations are carried out for $a = 0.1$ and $b = -0.4$ (the remaining data as before). Figure 14 shows the results of numerical simulations. In the figure of equivalent plastic strains some shear bands can be seen, however the load–displacement diagram does not show any instabilities in spite of some negative pivots monitored in the output. The explanation is provided by the analysis of the acoustic tensor. It is again examined for the plane strain compression at the onset of plastic yielding. The results depicted in Fig. 14 indicate that for the considered data a discontinuous bifurcation is possible already when yielding first occurs. Adopting a larger value of the gradient influence factor g does not stabilize the response.

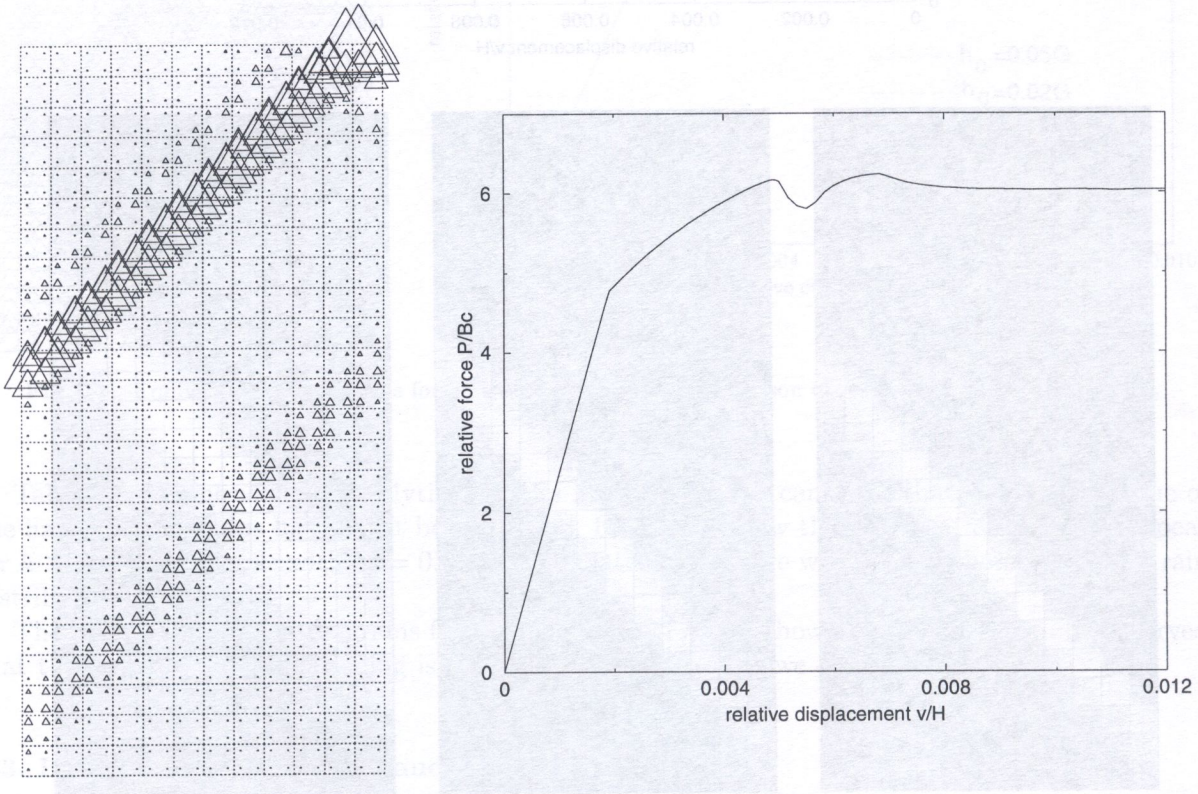

Fig. 13. Equivalent plastic strains and load–displacement diagram for a=0.5 b=-0.1

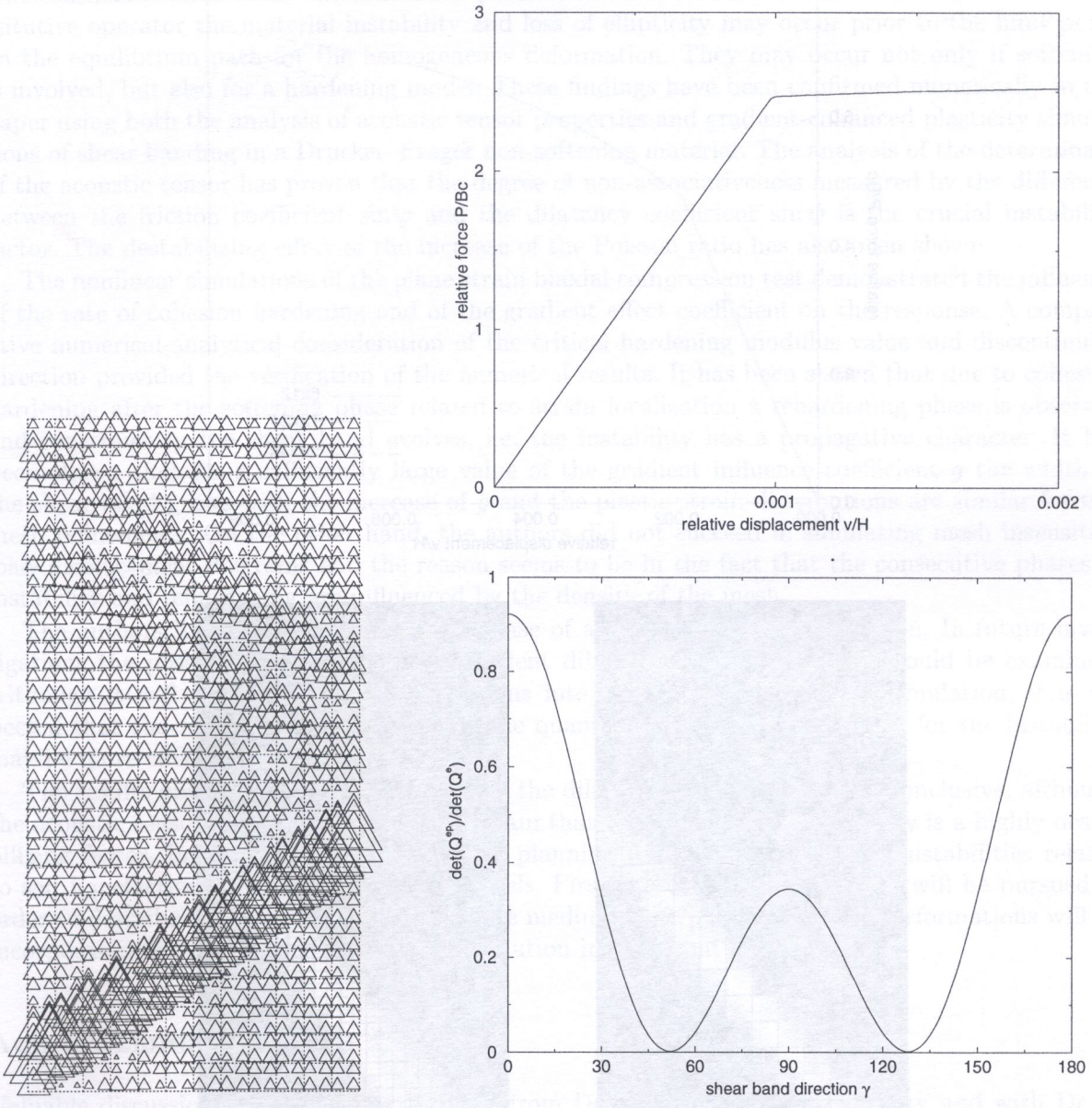

Fig. 14. Equivalent plastic strains, load–displacement diagram and analysis of $\mathbf{Q}^{ep}$ for a=0.1 and b=-0.4

4.5. Mesh sensitivity

If the classical continuum theory is used in presence of material instabilities triggering localization, the ellipticity of the governing partial differential equations is lost. Consequently, numerical results become determined by the discretization. The mesh-dependence is signalled by the fact that for different meshes the shear band always occupies the smallest possible area. The gradient-enhanced plasticity is used in our calculations to avoid this mesh-sensitivity. In order to check whether the applied regularization method prevents mesh-dependence we repeat the calculations with $a = 0.5$, $b = 0.0$, $g = 100N$ and $h_c = 0.0001G$ for three different meshes (6×12, 12×24, 24×48 elements). The results of computations are presented in Fig. 15. As can be seen, the load–displacement diagrams for different meshes show mesh-sensitivity. The diagram for the coarse mesh does not show any instabilities, for the fine mesh the response is much more brittle than for the medium one. On the other hand, strains do not localize in the smallest possible area and, moreover, the deforma-

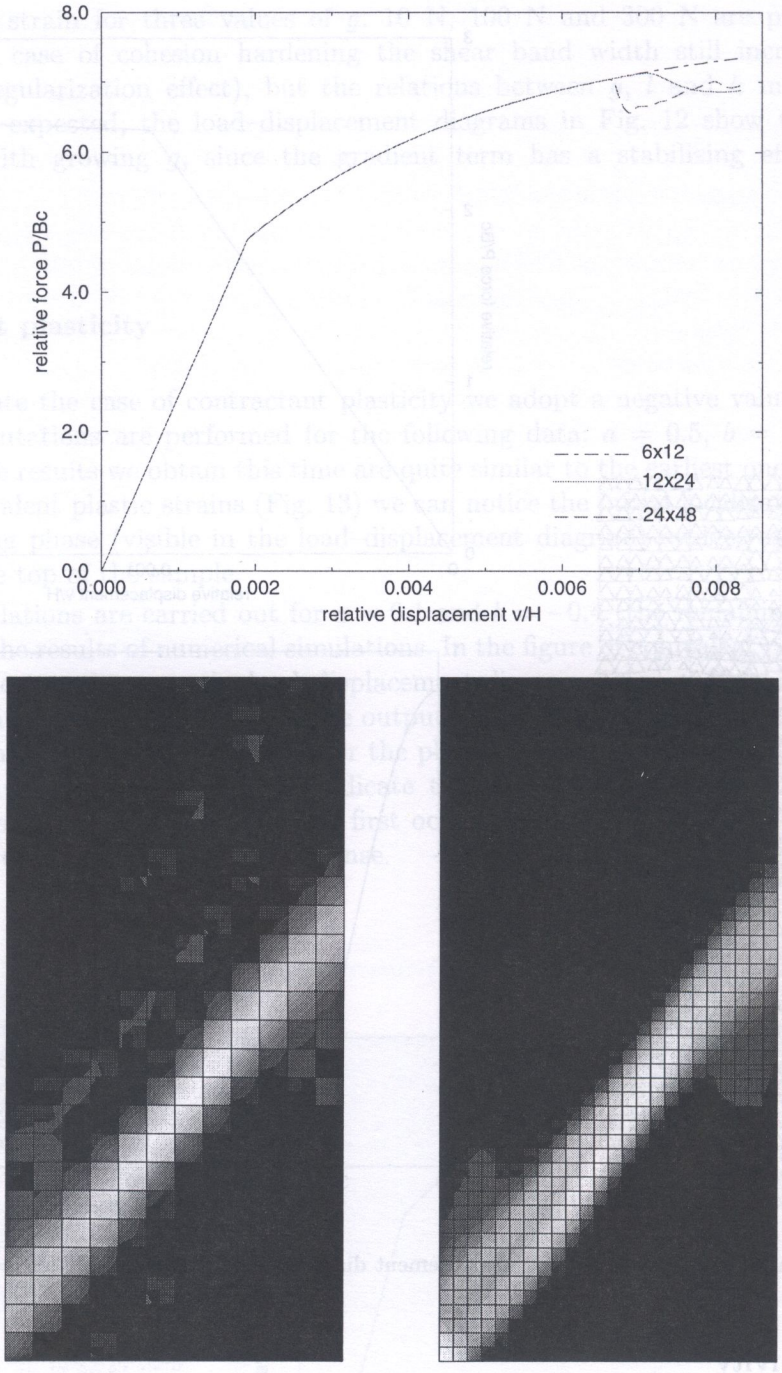

Fig. 15. Comparison of results for different meshes

tion patterns (plotted for the upper edge displacement $v = 1.0$ mm) and shear band widths are approximately the same for the medium and fine meshes. The figure of equivalent plastic strains for the first mesh (6×12) has been omitted in Fig. 15 since this mesh seems too coarse to give any reasonable results.

5. Final remarks

Theoretical considerations referred to in Section 3 can be summarized as follows. The occurrence of a material instability is a necessary condition for the loss of ellipticity, which is associated with

a discontinuous bifurcation and marks the possible onset of localization. For a non-symmetric constitutive operator the material instability and loss of ellipticity may occur prior to the limit point on the equilibrium path for the homogeneous deformation. They may occur not only if softening is involved, but also for a hardening model. These findings have been confirmed numerically in the paper using both the analysis of acoustic tensor properties and gradient-enhanced plasticity simulations of shear banding in a Drucker–Prager non-softening material. The analysis of the determinant of the acoustic tensor has proven that the degree of non-associativeness measured by the difference between the friction coefficient $\sin\varphi$ and the dilatancy coefficient $\sin\psi$ is the crucial instability factor. The destabilizing effect of the increase of the Poisson ratio has also been shown.

The nonlinear simulations of the plane strain biaxial compression test demonstrated the influence of the rate of cohesion hardening and of the gradient effect coefficient on the response. A comparative numerical-analytical consideration of the critical hardening modulus value and discontinuity direction provided the verification of the numerical results. It has been shown that due to cohesion hardening after the softening phase related to strain localization a rehardening phase is observed and consequently the shear band evolves, i.e. the instability has a propagative character. It has been shown that for a sufficiently large value of the gradient influence coefficient g the width of the shear band grows with the increase of g and the plastic strain distributions are similar for two mesh refinements. On the other hand, the authors did not succeed in simulating mesh insensitive load–displacement diagrams and the reason seems to lie in the fact that the consecutive phases of instability and rehardening are influenced by the density of the mesh.

The authors limited the analysis to the case of a gradient-enhanced cohesion. In future investigations the possibility of a gradient-dependent dilatancy or friction angle should be examined. Although it will introduce some modifications into the gradient plasticity formulation, it is expected that the regularization attached to the quantities which are responsible for the instability may be more effective.

The results obtained for negative values of the dilatancy angle have been inconclusive, although the acoustic tensor properties have proven again that the contractant plastic flow is a highly destabilizing factor. In the future the authors are planning to analyze the issue of instabilities related to soil liquefaction using more accurate models. Firstly, a consolidation theory will be pursued in order to describe the behaviour of a two-phase medium [4, 27]. Secondly, large deformations will be incorporated in order to take the density evolution into account [14].

Acknowledgments

Valuable discussions with Prof. R. de Borst from Delft University of Technology and with Dr A. Winnicki from Cracow University of Technology as well as the financial support of the Polish Committee for Scientific Research (grant PB 7 T07A 03612) are gratefully acknowledged. The computations have been performed with a pilot version of the DIANA finite element package.

References

[1] *DIANA Finite Element Analysis. User's Manual, Release 6.1.* Technical report, TNO Building and Construction Research, Delft, 1996.

[2] J.P. Bardet. Finite element analysis of plane strain bifurcation within compressible solids. *Comp. and Struct.*, **36**(6): 993–1007, 1990.

[3] J.P. Bardet. Analytical solutions for the plane-strain bifurcation of compressible solids. *ASME J. Appl. Mech.*, **58**: 651–657, 1991.

[4] J.P. Bardet. Plane-strain instability of saturated porous media. *ASCE J. Eng. Mech.*, **121**(6): 717–724, 1995.

[5] Z.P. Bažant and G. Pijaudier-Cabot. Nonlocal continuum damage, localization instability and convergence. *ASME J. Appl. Mech.*, **55**: 287–293, 1988.

[6] R. de Borst. *Non-linear analysis of frictional materials.* Ph.D. dissertation, Delft University of Technology, Delft, 1986.

[7] R. de Borst. Bifurcations in finite element models with a nonassociated flow law. *Int. J. Num. Anal. Meth. Geomech.*, **12**: 99–116, 1988.

[8] R. de Borst and H.-B. Mühlhaus. Gradient-dependent plasticity: Formulation and algorithmic aspects. *Int. J. Num. Meth. Eng.*, **35**: 521–539, 1992.

[9] R. de Borst and J. Pamin. Some novel developments in finite element procedures for gradient-dependent plasticity. *Int. J. Num. Meth. Eng.*, **39**: 2477–2505, 1996.

[10] R. de Borst, L.J. Sluys, H.-B. Mühlhaus, and J. Pamin. Fundamental issues in finite element analyses of localization of deformation. *Eng. Comput.*, **10**: 99–121, 1993.

[11] R. de Borst and E. van der Giessen, eds. *Material Instabilities in Solids.* IUTAM, Chichester, John Wiley & Sons, 1998.

[12] J. Desrues. Localisation patterns in ductile and brittle geomaterials. In: [11], pp. 137–158.

[13] R. Hill. A general theory of uniqueness and stability in elastic-plastic solids. *J. Mech. Phys. Solids*, **6**: 236–249, 1958.

[14] T. Łodygowski. Theoretical and numerical aspects of plastic strain localization. Technical Report 312, Poznań University of Technology, Poznań, 1996.

[15] G. Maier and T. Hueckel. Nonassociated and coupled flow rules of elastoplasticity for rock-like materials. *Int. J. Rock Mech. Min. Sci. and Geomech. Abstr.*, **16**: 77–92, 1979.

[16] H.-B. Mühlhaus and E.C. Aifantis. A variational principle for gradient plasticity. *Int. J. Sol. Struct.*, **28**: 845–857, 1991.

[17] H.-B. Mühlhaus and I. Vardoulakis. The thickness of shear bands in granular materials. *Geotechnique*, **37**: 271–283, 1987.

[18] M.K. Neilsen and H.L. Schreyer. Bifurcations in elastic-plastic materials. *Int. J. Sol. Struct.*, **30**: 521–544, 1993.

[19] M. Ortiz, Y. Leroy, and A. Needleman. A finite element method for localized failure analysis. *Comp. Meth. Appl. Mech. Eng.*, **61**: 189–214, 1987.

[20] N.S. Ottosen and K. Runesson. Properties of discontinuous bifurcation solutions in elasto-plasticity. *Int. J. Sol. Struct.*, **27**(4): 401–421, 1991.

[21] J. Pamin. *Gradient-Dependent Plasticity in Numerical Simulation of Localization Phenomena.* Ph.D. dissertation, Delft University of Technology, Delft, 1994.

[22] J. Pamin and R. de Borst. A gradient plasticity approach to finite element predictions of soil instability. *Arch. Mech.*, **47**: 353–377, 1995.

[23] B. Raniecki and O.T. Bruhns. Bounds to bifurcation stresses in solids with non-associated plastic flow law with finite strain. *J. Mech. Phys. Solids*, **29**(2): 153–172, 1981.

[24] J.W. Rudnicki and J.R. Rice. Conditions for the localization of deformation in pressure-sensitive dilatant materials. *J. Mech. Phys. Solids*, **23**: 371–394, 1975.

[25] K. Runesson and Z. Mróz. A note on nonassociated plastic flow rules. *Int. J. Plasticity*, **5**: 639–658, 1989.

[26] K. Runesson, N.S. Ottosen, and D. Perić. Discontinuous bifurcations of elastic-plastic solutions at plane stress and plane strain. *Int. J. Plasticity*, **7**: 99–121, 1989.

[27] B.A. Schrefler, L. Sanavia, and C.E. Majorana. A multiphase medium model for localisation and postlocalisation simulation in geomechanics. *Mech. Cohes.-frict. Mater.*, **1**: 95–114, 1996.

[28] L.J. Sluys. *Wave Propagation, Localization and Dispersion in Softening Solids.* Ph.D. dissertation, Delft University of Technology, Delft, 1992.

[29] H. van der Veen. *The Significance and Use of Eigenvalues and Eigenvectors in the Numerical Analysis of Elasto-Plastic Soils.* Ph.D. dissertation, Delft University of Technology, Delft, 1998.

[30] I. Vardoulakis and E.C Aifantis. Gradient dependent dilatancy and its implications in shear banding and liquefaction. *Ing.-Arch.*, **59**: 197–208, 1989.

[31] I. Vardoulakis and E.C. Aifantis. A gradient flow theory of plasticity for granular materials. *Acta Mechanica*, **87**: 197–217, 1991.

[32] I. Vardoulakis and J. Sulem. *Bifurcation Analysis in Geomechanics.* Blackie Academic & Professional, London, 1995.

[33] P.A. Vermeer and R. de Borst. Non-associated plasticity for soils, concrete and rock. *Heron*, 29(3), 1984.

[34] K. Willam and M. Iordache. Fundamental aspects of failure modes in brittle solids. In: Z.P. Bažant et al., eds., *Fracture and Damage in Quasibrittle Structures*, pp. 53–66. London, E&FN Spon, 1994.

[35] K.J. Willam and A. Dietsche. Fundamental aspects of strain-softening descriptions. In: Z.P. Bažant, ed., *Fracture Mechanics of Concrete Structures*, pp. 227–238. London–New York, FRAMCOS, Elsevier Applied Science, 1992.

[36] K.J. Willam and G. Etse. Failure assessment of the extended Leon model for plain concrete. In: N. Bićanić et al., eds., *Proc. Second Int. Conf. Computer Aided Analysis and Design of Concrete Structures*, pp. 851–870. Swansea, Pineridge Press, 1990.

[37] T. Yoshida, F. Tatsuoka, M.S.A. Siddiquee, Y. Kamegai, and C.-S. Park. Shear banding in sands observed in plane strain compression. In: R. Chambon, J. Desrues, I. Vardoulakis, eds., *Localisation and bifurcation theory for soils and rocks*, pp. 165–179. Rotterdam/Brookfield, A.A. Balkema, 1994.